JOURNAL OF VIROLOGY, Sept. 2005, p. 12065–12076 Vol. 79, No. 18
0022-538X/05/$08.00+0 doi:10.1128/JVI.79.18.12065–12076.2005

Membrane Structures of the Hemifusion-Inducing Fusion Peptide Mutant G1S and the Fusion-Blocking Mutant G1V of Influenza Virus Hemagglutinin Suggest a Mechanism for Pore Opening in Membrane Fusion

Yinling Li, Xing Han,† Alex L. Lai, John H. Bushweller, David S. Cafiso, and Lukas K. Tamm*

Department of Molecular Physiology and Biological Physics, University of Virginia, Charlottesville, Virginia

Received 6 May 2005/Accepted 21 June 2005

Influenza virus hemagglutinin (HA)-mediated membrane fusion is initiated by a conformational change that releases a V-shaped hydrophobic fusion domain, the fusion peptide, into the lipid bilayer of the target membrane. The most N-terminal residue of this domain, a glycine, is highly conserved and is particularly critical for HA function; G1S and G1V mutant HAs cause hemifusion and abolish fusion, respectively. We have determined the atomic resolution structures of the G1S and G1V mutant fusion domains in membrane environments. G1S forms a V with a disrupted "glycine edge" on its N-terminal arm and G1V adopts a slightly tilted linear helical structure in membranes. Abolishment of the kink in G1V results in reduced hydrophobic penetration of the lipid bilayer and an increased propensity to form β-structures at the membrane surface. These results underline the functional importance of the kink in the fusion peptide and suggest a structural role for the N-terminal glycine ridge in viral membrane fusion.

Enveloped viruses enter and infect animal cells by fusing their own membrane with the plasma or an internal membrane of target cells after appropriate receptor recognition. Highly specialized viral membrane proteins catalyze the recognition and fusion process, and the structures of the soluble domains of many viral fusion proteins and fragments of fusion proteins have been solved by X-ray crystallography (17, 22, 41, 45, 46). Viral fusion proteins can be classified according to their structures into classes I and II. Class I fusion proteins are characterized by trimeric helical bundles, whereas class II fusion proteins form lattices of dimers of β-sheet-rich proteins on the viral surfaces.

The structurally and functionally best-characterized class I fusion protein is the hemagglutinin (HA) of influenza virus. Therefore, it has become the prototypic system to study mechanisms of viral membrane fusion (16, 31). Influenza virus enters cells by receptor-mediated endocytosis and subsequent fusion of the viral and endosomal membranes triggered by the pH ~5 environment in the endosome. Influenza virus HA is a complex of six polypeptide chains with the stoichiometry $(HA1/HA2)_3$. The HA2 transmembrane subunits bear the major responsibility for membrane fusion. Upon exposure to pH 5, HA2 undergoes a massive conformational change (6, 52), which results in exposure of the hydrophobic "fusion domain" at the N terminus. Because energy is released, this conformational change has been described as spring-loaded (8). A second conformational change reverses the direction of the C terminus and brings it into close proximity to the N terminus of the postfusion structure of the ectodomain (9).

Although structural studies of the soluble domains of HA2 have yielded many insights into the "engine" that drives membrane fusion, they provided little information on how the released energy is transmitted into the membrane and how the "handles" of this machine shape the membranes into fusion-competent structures. This task falls to the fusion and transmembrane (TM) domains of HA2. The fusion and TM domains are not present in the crystal structures of the fusogenic conformations of HA or any other viral fusion protein.

Fusion domains have highly conserved, very hydrophobic, and glycine-rich sequences (14, 42, 47). Even conservative single-site mutations in these sequences can impair or completely eliminate the fusion activity of fusion proteins. Several mutagenesis studies indicate that the glycine at the extreme N terminus of HA2 is particularly critical in determining the fusion phenotype of influenza virus HA (10, 21, 36, 43). The only tolerated change in this position appears to be a mutation of Gly-1 to an alanine. Changes to more polar or more hydrophobic residues result in a complete loss of activity. A particularly interesting mutant is G1S, because replacing Gly-1 with a serine facilitates lipid mixing but not contents mixing (43). This behavior is the hallmark of "hemifusion," i.e., an intermediate state in which the contacting lipid monolayers are believed to be merged but the distal lipid monolayers are still intact and separated (10, 36).

We have recently determined the atomic structures and an associated pH-dependent conformational change of the fusion domain of influenza virus HA in lipid bilayers using a combined nuclear magnetic resonance (NMR) and electron paramagnetic resonance (EPR) approach (26). The fusion domain adopts a V-shaped structure with a kink around Asn-12. The

* Corresponding author. Mailing address: Department of Molecular Physiology and Biological Physics, University of Virginia, Health Sciences Center, P.O. Box 800736, Charlottesville, VA 22908-0736. Phone: (434) 982-3578. Fax: (434) 982-1616. E-mail: lkt2e@virginia.edu.

† Present address: DuPont Haskell Laboratory for Health and Environmental Sciences, Newark, DE 19714.

N-terminal arm of the V is α-helical with a glycine ridge on the outer surface. The C-terminal arm is also helical at pH 5 but not at pH 7. The binding of the fusion domains of the critical fusion mutants G1S and G1V to lipid bilayers has been measured by isothermal titration calorimetry and fluorescence and has been compared to that of the wild-type fusion domain (33). The free energy and enthalpy of binding of G1V were significantly reduced compared to those of the wild-type and G1S, which were similar to one another.

In the present work, we determined the structures of the G1S and G1V mutants in detergent micelles by NMR and measured the dispositions of these structures in lipid bilayers by spin-label EPR and attenuated total reflection Fourier transform infrared (ATR-FTIR) spectroscopy. The differences between G1S and the wild type were subtle and local, whereas the G1V mutation induced global structural changes that were evident by all three spectroscopic methods and in different model membranes. The results provide the first structural evidence for the hemifusion intermediate in any fusion domain and suggest a mechanism of how functional fusion domains interact with target membranes in the course of membrane fusion.

MATERIALS AND METHODS

Peptides. All peptides were synthesized by solid-phase synthesis in the Biomolecular Research Facility at the University of Virginia using 9-fluorenylmethoxy carbonyl chemistry. Reverse-phase high-pressure liquid chromatography-purified peptides were >96% pure, and their molecular masses were confirmed by mass spectrometry. Concentrations of stock solutions were determined by quantitative amino acid analysis.

Liposomes. Small unilamellar vesicles were prepared by mixing four parts of 1-palmitoyl-2-oleoyl-3-*sn*-phosphatidylcholine (POPC) and one part of 1-palmitoyl-2-oleoyl-3-*sn*-phosphatidylglycerol (POPG) (Avanti Polar Lipid, Alabaster, AL) in chloroform, evaporating the solvent under a stream of nitrogen, rehydrating and vortexing the lipid dispersions in 5 mM HEPES, 10 mM morpholineethanesulfonic acid (MES) buffer, pH 5, followed by sonication with a probe sonicator for 30 min at 50% duty cycle on ice. Phospholipid concentrations were determined by phosphorus assay (2). Large unilamellar vesicles (100 nm in diameter) of the same lipid composition were prepared by extrusion through polycarbonate membranes as described (27).

NMR spectroscopy. NMR measurements were carried out at 30°C on a Varian Innova 600-MHz NMR spectrometer. The samples contained 2 mM peptide, 400 mM d_{38}-dodecylphosphocholine in 0.05% NaN_3, 5 mM dithiothreitol, 20 mM d_4-acetic acid, pH 5 buffer (95% H_2O/5% deuterium oxide). Resonances were assigned from total correlated spectroscopy (TOCSY) and nuclear Overhauser effect spectroscopy (NOESY) spectra with 56- and 80-ms mixing times, respectively. Nuclear Overhauser enhancement (NOE) upper distance constraints were determined from NOESY spectra with a mixing time of 80 ms.

Spin-label EPR spectroscopy. Continuous-wave power saturation EPR measurements were performed with a Varian E-line Century Series EPR spectrometer with a two-loop, one-gap X-band resonator. The samples contained 100 μM spin-labeled peptide bound to extruded large unilamellar lipid vesicles (POPC:POPG, 4:1) at a total phospholipid concentration of 100 mM in 5 mM HEPES, 10 mM MES, pH 7.4 or 5. Power saturation curves were obtained from the peak-to-peak amplitude of the central ($M = 0$) line of the first derivative EPR spectra under three conditions: equilibrated with N_2, equilibrated with air, and equilibrated with N_2 in the presence of 20 mM Ni-ethylenediamine-*N*,*N*′-diacetic acid (EDDA). The depth of the spin label in the membrane was derived from the depth parameter $\Phi = \ln\{[P_{1/2}(O_2) - P_{1/2}(N_2)]/[P_{1/2}(\text{NiEDDA}) - P_{1/2}(N_2)]\}$ (1), which was calibrated with 0.1% of spin-labeled phosphatidylcholines in POPC:POPG (4:1) bilayers with doxyl nitroxides in positions 5, 7, 10, and 12 along the *sn*-2 alkyl chain (12).

ATR-FTIR spectroscopy. The ATR-FTIR spectra of peptides bound to planar phospholipid bilayers of 1,2-myristoyl-3-*sn*-phosphatidylcholine/POPC:POPG (4:1) supported on germanium ATR plates and in 5 mM HEPES, 10 mM MES, pH 5, buffer were recorded on a Bruker Vector 22 Fourier transform infrared spectrometer. Experimental procedures and data evaluation were as described (29). Average orientations of the peptides in lipid bilayers were determined from the dichroic ratios of the amide I′ bands and the resulting order parameters which are defined as $S = \langle 3\cos^2\theta - 1\rangle/2$, where θ is the angle from the membrane normal and the angle brackets denote an ensemble average of all angles present in the sample (48).

Structure calculation. Structures were calculated with the program DYANA (25). The input consisted of the NOE upper distance constraints and dihedral angle constraints derived from the program HABAS (24). Following the torsion angle dynamics calculations, the 20 conformers with the lowest target function values were subjected to energy minimization using the AMBER force field implemented in the program OPAL (34). The resulting 20 energy-minimized conformers were used to represent the structures of G1S and G1V in dodecylphosphocholine (DPC) micelles at pH 5.

Docking of NMR structures to lipid bilayers. A preconstructed 1-oxyl-2,2,5,5-tetramethyl-Δ^3-pyrroline-3-methyl (MTSSL) structure was inserted with the program InsightII into the NMR structures at the three labeled sites. The dihedral angles χ_1 and χ_2 of the spin label were set to 300° to match the dominant conformation observed for the MTSSL-derivatized cysteine in proteins (32). The structures were then docked by least-squares analysis to the experimentally measured Φ parameters until the best agreement between model and experiment was obtained. A POPC bilayer simulated by molecular dynamics (50) was used to represent the membrane.

Protein structure accession numbers. Coordinates G1S and G1V have been deposited in the Protein Data Bank under accession numbers 1XOO and 1XOP, respectively.

RESULTS

Fusion domains were synthesized as "host-guest" peptides with single-site mutations in position 1 (33). We showed previously that the host-guest concept makes it possible to bind fusion domains to membranes under physiological conditions and that these domains mediate pH-dependent lipid mixing and hemolysis of red blood cells as do their full-length HA counterparts (28). We also showed previously that wild-type, G1S, and G1V fusion domains bound to lipid bilayers at pH 5 have significant α-helical content (33). The circular dichroism spectra of wild-type and G1S fusion domains in lipid bilayers were very similar to one another, but G1V exhibited a spectrum that was indicative of a lower helical content. Very similar spectra were obtained in DPC micelles (data not shown).

Structures of G1S and G1V in detergent micelles. We recently solved by NMR the structure of the wild-type fusion domain in DPC micelles. Site-directed spin labeling further showed that the same structure is present in lipid bilayers (26). We have now solved the NMR structures of G1S and G1V in DPC micelles at pH 5. Backbone and side chain resonances were assigned based on TOCSY and NOESY spectra recorded at 600 MHz (Table 1). Figure 1 shows the amide proton (HN) and α-carbon proton (Hα) chemical shift differences between the mutant and the wild-type fusion domains. Chemical shift differences from random coil chemical shifts of backbone protons are highly indicative of polypeptide secondary structure (53). The differences between the mutant and wild-type fusion domains are greatest at the N terminus, but significant differences are seen to extend deeply into the fusion domain structure. Despite the obvious differences between the three peptides, the differences of the Hα (HN) chemical shifts from the random coil values are still negative (positive), indicative of stable helical structures of the N-terminal halves of each molecule.

NMR structures are usually calculated from a large number of proton-proton distances that are determined from nuclear Overhauser enhancement measurements between protons that

TABLE 1. Chemical shifts and assignments of backbone and side chain protons of wild-type, G1S, and G1V fusion domains in DPC micelles at pH 5.0[a]

Fusion domain	Residue	HN	Hα	Hβ	Others
Wild type	G1	8.164	3.979		
			3.907		
	L2	9.385	4.078	1.682	δCH3, 0.923, 0.833
				1.561	
	F3	8.979	4.198	3.191	2,6H, 7.250
				3.119	
	G4	8.516	3.739		
	A5	8.160	4.243	1.525	
	I6	8.139	3.736	1.958	γCH2, 1.886, 1.051; γCH3, 0.924; δCH3, 0.820
	A7	8.526	3.890	1.331	
	G8	8.169	3.818		
			3.734		
	F9	7.926	4.424	3.254	3,5H, 7.214; 2,6H, 7.179
	I10	8.195	3.644	2.022	γCH2, 1.893, 1.250; γCH3, 0.924; δCH3, 0.855
	E11	8.341	4.014	2.108	γCH2, 2.518, 2.383
	N12	8.169	4.573	2.737	δNH2, 7.620, 6.877
	G13	8.248	3.940		
	W14	8.455	4.376	3.317	εNH, 10.490; 4H, 7.470; 7H, 7.422; 2H, 7.254; 6H, 7.046; 5H, 6.923
	E15	8.342	3.901	2.057	γCH2, 2.326
	G16	7.913	3.909		
			3.793		
	M17	7.866	4.337	2.066	γCH2, 2.545, 2.464
	I18	7.719	4.018	1.794	γCH2, 1.262, 1.071; γCH3, 0.751; δCH3, 0.693
	D19	8.174	4.562	2.726	
	G20	8.387	3.986		
G1S	S1	9.565	4.483	4.320	
				4.109	
	L2	9.564	4.169	1.701	δCH3, 0.912, 0.842
				1.610	
	F3	8.789	4.164	3.129	2,6H, 7.222
				3.064	
	G4	8.182	3.997		
			3.887		
	A5	8.117	4.227	1.543	
	I6	8.042	3.711	1.931	γCH2, 1.861, 1.036; γCH3, 0.910; δCH3, 0.805
	A7	8.483	3.870	1.313	
	G8	8.141	3.874		
			3.795		
	F9	7.910	4.410	3.240	3,5H, 7.195; 2,6H, 7.162
	I10	8.159	3.631	2.007	γCH2, 1.880, 1.235; γCH3, 0.907; δCH3, 0.840
	E11	8.325	4.000	2.091	γCH2, 2.484, 2.354
	N12	8.147	4.559	2.730	δNH2, 7.591, 6.853
	G13	8.147	3.708		
	W14	8.435	4.364	3.296	εNH, 10.468; 4H, 7.449; 7H, 7.397; 2H, 7.236; 6H, 7.018; 5H, 6.897
	E15	8.319	3.884	1.992	γCH2, 2.303
	G16	7.903	3.885		
			3.771		
	M17	7.848	4.316	2.044	γCH2, 2.526, 2.442
	I18	7.700	4.001	1.778	γCH2, 1.250, 1.061; γCH3, 0.741; δCH3, 0.679
	D19	8.151	4.557	2.708	
	G20	8.266	3.967		
G1V	V1	8.967	3.780	2.201	γCH3, 1.103, 0.936
	L2	8.942	4.280	1.663	δCH3, 0.903, 0.845
				1.578	
	F3	8.899	4.222	3.187	2,6H, 7.236
				3.133	
	G4	8.658	3.955		
			3.764		
	A5	7.929	4.262	1.493	
	I6	7.835	3.786	1.969	γCH2, 1.735, 1.092; γCH3, 0.911; δCH3, 0.827
	A7	8.299	3.898	1.339	
	G8	8.103	3.873		
			3.800		
	F9	7.850	4.397	3.236	3,5H, 7.205; 2,6H, 7.177
	I10	8.082	3.653	2.006	γCH2, 1.853, 1.232; γCH3, 0.908; δCH3, 0.841
	E11	8.299	3.997	2.092	γCH2, 2.476, 2.351
	N12	8.144	4.558	2.730	δNH2, 7.590, 6.854
	G13	8.149	3.698		
	W14	8.435	4.359	3.306	εNH, 10.468; 4H, 7.441; 7H, 7.394; 2H, 7.231; 6H, 7.018; 5H, 6.897
	E15	8.312	3.873	1.993	γCH2, 2.307
	G16	7.893	3.878		
			3.774		
	M17	7.831	4.303	2.043	γCH2, 2.523, 2.443
	I18	7.673	3.997	1.769	γCH2, 1.233, 1.051; γCH3, 0.729; δCH3, 0.668
	D19	8.138	4.553	2.709	
	G20	8.223	3.920		

[a] Chemical shifts are given in parts per million.

are in close spatial proximity. From a total of 467 and 492 assigned NOE cross-peaks, 145 and 136 nonredundant upper limit constraints were obtained for G1S and G1V, respectively (Table 2). A total of 53 (G1S) and 56 (G1V) dihedral angle constraints were also included in the structure calculation (Table 2). The backbone structures of the 20 lowest-energy conformers of G1S and G1V in DPC micelles at pH 5 are shown in blue in Fig. 2A and B, respectively. We calculated 100 structures for both peptides. In the case of G1V, the 25 lowest-energy conformers fall into two classes: 20 structures (class I) exhibit a single helix as shown in panels B, D, F, and G of Fig. 2. Five structures (class II) exhibit a small bend at residues 6 and 7, but otherwise superimpose well onto the class I structures. The average energy minimum of class I structures is marginally lower (–242 ± 21 kcal/mol) than the average energy minimum of class II structures (–223 ± 21 kcal/mol).

To highlight the structural differences between the mutant and wild-type peptides, the "most typical" (i.e., closest to the mean) conformer of the wild-type peptide at pH 5 is superimposed in red on the family of G1S and G1V structures. Ribbon representations of the most typical conformers of the G1S, G1V, and wild-type peptides are shown in Fig. 2C, D, and E, respectively. The experimentally determined side chain conformations are also included in these figures as indicated. Electrostatic surface potential representations of the wild-type, G1S, and G1V peptide structures are shown in Fig. 2G. They

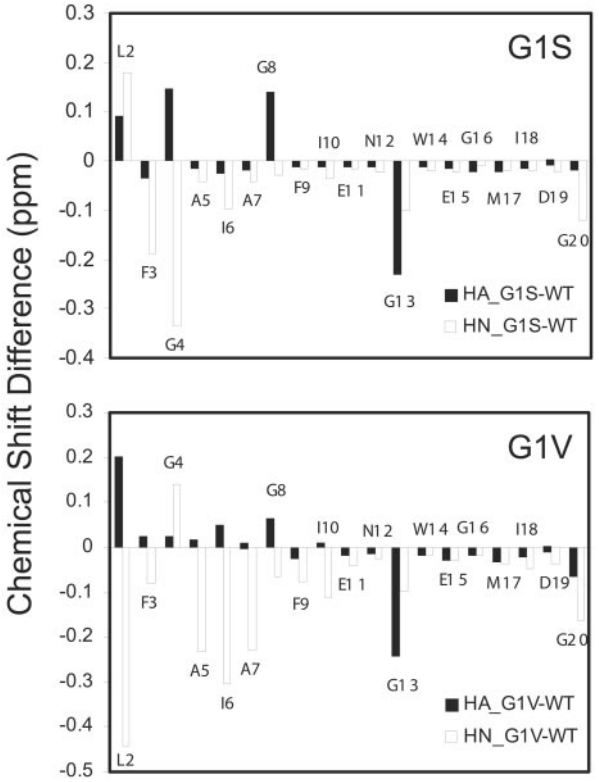

FIG. 1. Backbone ^{1}H chemical shift differences indicating structural differences between mutant and wild-type fusion domains bound to DPC micelles at pH 5. A, Differences between G1S and wild-type fusion domains. B, Differences between G1V and wild-type fusion domains.

clearly show the amphipathic nature of all three molecules with hydrophobic bottom and more hydrophilic top faces.

The overall shape of G1S resembles that of the wild-type peptide. Both molecules form a shallow-angle inverted V. G1S has an N-terminal α-helix that extends from Leu 2 to Asn 12, a break at Gly 13 and Trp 14, and a short 3_{10}-helix between Glu 15 and Ile 18. As in the wild-type peptide, the kink in the middle of G1S is defined by distance constraints derived from NOEs between Hα of Ile 10 and HN of Trp 14 and between Hα of Ile 10 and Hε3 of Trp 14 (shown as an example in Fig. 3B), several backbone short-range NOE distance constraints, and several chemical shift-derived angle constraints. The kinked amphipathic structure ensures an oblique insertion of the two arms of the V with all hydrophobic residues penetrating deeply into the lipid bilayer (26).

Upon closer inspection, it is seen that the kinks of the wild-type and G1S peptides are slightly different. The N-terminal helix of G1S extends a little further into the kink than that of the wild-type peptide. This is reflected, for example, in chemical shift differences of Hα and HN resonances of Gly 13 (Table 1 and Fig. 1) and differences of NOEs between HN of Gly 13 and HN of Trp 14, which is absent in the wild-type but present in the G1S peptide. A second subtle difference is that the N-terminal helix of G1S is more distorted than that of the wild-type peptide. The NOE from the N-terminal Hα to the HN of Phe 3 is strong in G1S (Fig. 3E), but very weak in the wild-type peptide (Fig. 3D). The N-terminal end of G1S but not of the wild-type peptide is overwound. This distortion is due to the formation of a hydrogen bond from the backbone NH of Gly 4 to the side chain Oγ of Ser 1, which forces the backbone NH of Ala 5 rather than Gly 4 to hydrogen bond to the backbone CO of Ser 1. This causes the side chain of Ser 1 of G1S to point upwards and disrupt a smooth "glycine edge" that is formed by Gly 1, Gly 4, and Gly 8 at the top of the N-terminal arm of the wild-type structure.

TABLE 2. Structural statistics of the NMR structures of G1S and G1V

Parameter	G1S	G1V
Target function (Å)	0.21 ± 0.03	0.13 ± 0.05
Experimental NMR constraints		
NOE distance constraints	145	136
Intraresidue	50	42
Sequential	48	57
Medium range	47	37
Long range	0	0
Angle constraints (derived from HABAS)	53	56
ϕ	19	19
ψ	16	16
χ^1	11	11
χ^2	9	10
NMR constraint violations		
NOE constraint violations		
Sum (Å)	2.57 ± 0.18	1.76 ± 0.20
Maximum (Å)	0.09 ± 0.01	0.10 ± 0.01
Angle constraint violations		
Sum (°)	3.52 ± 0.76	1.28 ± 1.42
Maximum (°)	2.12 ± 0.36	0.79 ± 0.67
AMBER energy (kcal/mol)	−171.3 ± 7.6	−241.6 ± 21.4
Root mean squared deviation from the mean structure (Å)		
Backbone atoms of all residues 1–20	1.21 ± 0.49	1.76 ± 0.41
All heavy atoms of all residues 1–20	1.60 ± 0.46	2.42 ± 0.44
Backbone atoms of residues 2–18	0.63 ± 0.28	1.06 ± 0.36
All heavy atoms of residues 2–18	1.14 ± 0.32	1.87 ± 0.49
Ramachandran statistics analyzed using PROCHECK-NMR		
Residues in allowed regions (%)	100.0	100.0
Residues in disallowed regions (%)	0.0	0.0

The structure of G1V in DPC micelles is quite different from the other two structures. Rather than forming a V, G1V adopts a linear amphipathic helical structure. The different structure of G1V is determined by quite significant differences of ϕ and ψ angle constraints that are derived from the different chemical shifts of the two molecules (Table 1, Fig. 1) and several medium-range NOE differences. For example, the NOEs between backbone and side chain protons of Ile 10 and Trp 14 (Hα–Hε3, Hα–HN), which contribute to constraining the structures of the wild-type and G1S peptides to the V's, are missing in the NOESY spectrum of G1V as shown in Fig. 3A, B, and C. In addition, many backbone short-range NOEs in this region are different among the three molecules and therefore define a turn in the wild-type and G1S but not in the G1V peptide. For

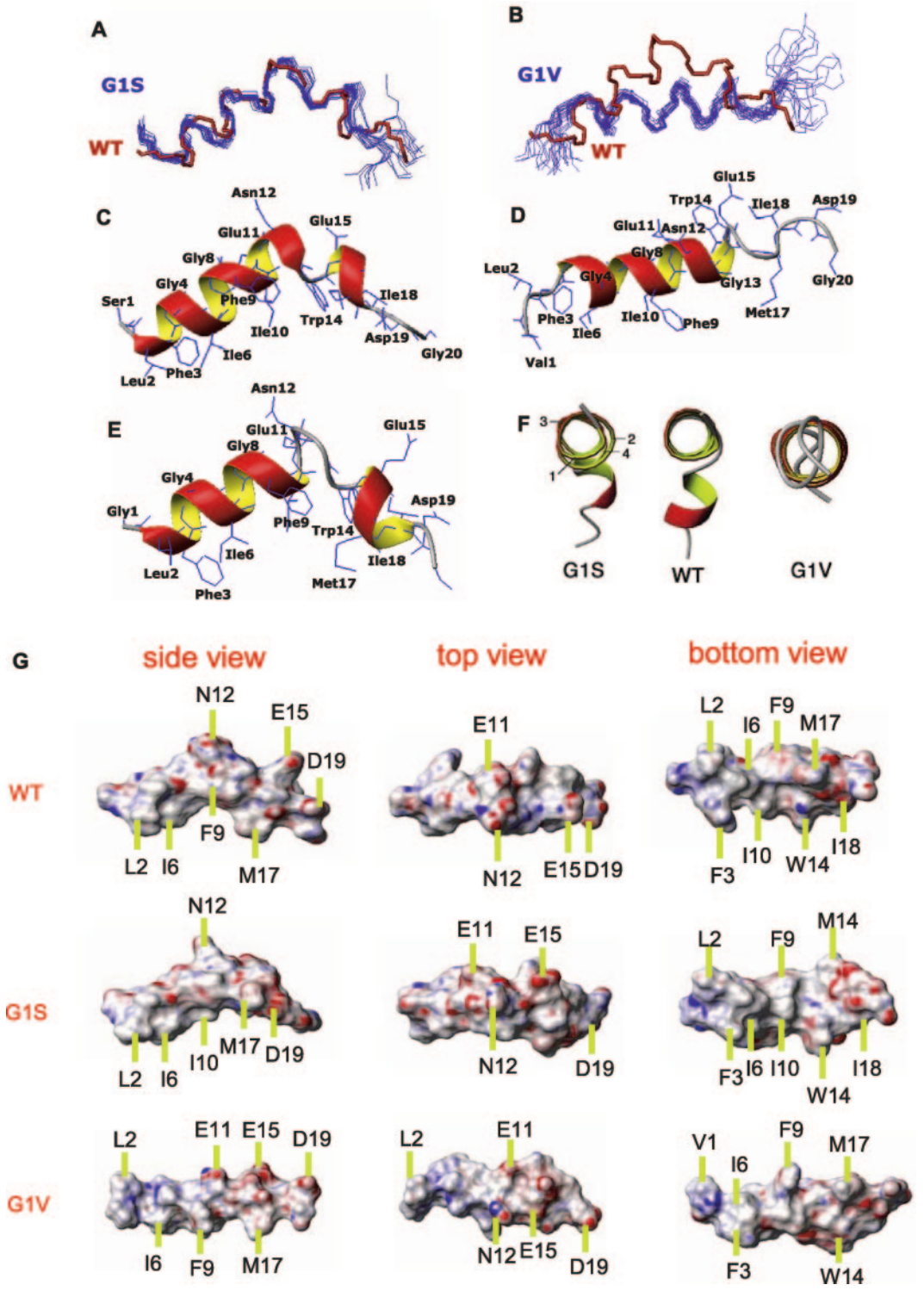

FIG. 2. Structures of G1S, G1V, and wild-type fusion domains in DPC micelles determined at pH 5 by ^{1}H-NMR spectroscopy. (A) 20 conformers representing the structure of G1S are shown in blue. For comparison, the "most typical" conformer of the wild-type fusion domain is superimposed in red on the family of G1S conformers. (B) Twenty conformers representing the structure of G1V are shown in blue. For comparison, the "most typical" conformer of the wild-type fusion domain is superimposed in red on the family of G1V conformers. (C) Ribbon representation of the closest-to-the-mean conformer of the G1S structure with side chains inserted. (D) Ribbon representation of the closest-to-the-mean conformer of the G1V structure with side chains inserted. (E) Ribbon representation of the closest-to-the-mean conformer of the wild-type structure with side chains inserted. (F) End-on views of the N-terminal helices of wild-type, G1S, and G1V fusion domains. The first, second, third, and fourth turns of the G1S helix are labeled. (G) GRASP (44)-generated electrostatic surface potential representations of the structures of wild-type, G1S, and G1V fusion domains at pH 5. Negative, positive, and neutral potentials are shown in red, blue, and white, respectively. Side, top, and bottom views are shown for each structure, and several residues are labeled for reference.

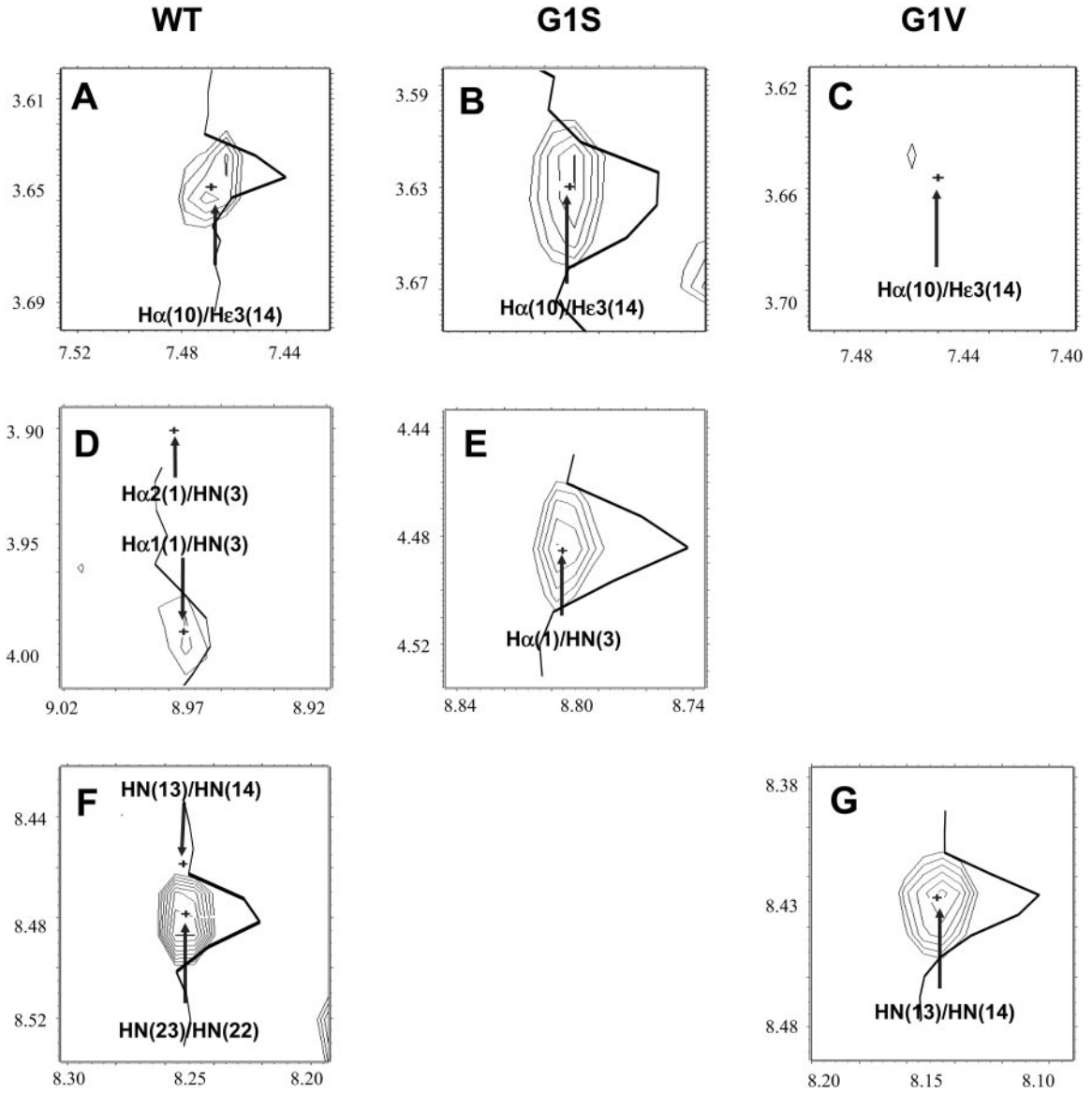

FIG. 3. Sections of NOESY spectra comparing NOEs that contribute to the definition of the different structures observed for the wild-type (WT), G1S, and G1V fusion domains in DPC micelles at pH 5. (A to C) NOE between Hα of Ile 10 and He3 of Trp 14 is present in the wild-type and G1S but absent in the G1V structure. (D to E) NOE between N-terminal Hα and HN of Phe 3 is present in G1S but very weak in the wild-type structure. (F to G) NOE between HN of Gly 13 and HN of Trp 14 is present in G1V but absent in the wild-type structure. All spectra were obtained under the same conditions and are plotted at the same contour level in each row. The thicker black lines are one-dimensional sections through the spectra at the positions of the indicated peaks.

example, the NOE between the HN of Gly 13 and HN of Trp 14 is strong in G1V (Fig. 3G), but absent in the wild-type peptide (Fig. 3F). Finally, many side chain NOEs are different between the wild-type and G1V peptides in both halves of these structures. In conclusion, the sum of these many different constraints results in an irregular linear helical structure of G1V that extends from Phe 3 to Ile 18, as shown in Fig. 2B, D, F, and G.

Disposition of G1S and G1V in the lipid bilayer. We previously showed by site-directed spin labeling that the wild-type fusion domain inserts into membranes with its apex positioned at the polar head group level of the lipid bilayer (26). We now used the same technology to measure the disposition of G1S and G1V in lipid bilayers. The two peptides were each synthesized with individual Cys substitutions in positions 3, 11, and 18 and labeled with the nitroxide spin label MTSSL in these positions. These positions were selected because they should define the approximate position of the fusion domains in the membrane and they should also indicate whether or not their structures are kinked in lipid bilayers. Power saturation EPR spectra were recorded for each of these peptides bound to lipid bilayers composed of POPC:POPG (4:1) in the presence of N_2, O_2, and NiEDDA. This method allows one to determine the depth of the nitroxide group in the lipid bilayer with a precision of approximately ± 2 Å as is described in more detail elsewhere (1).

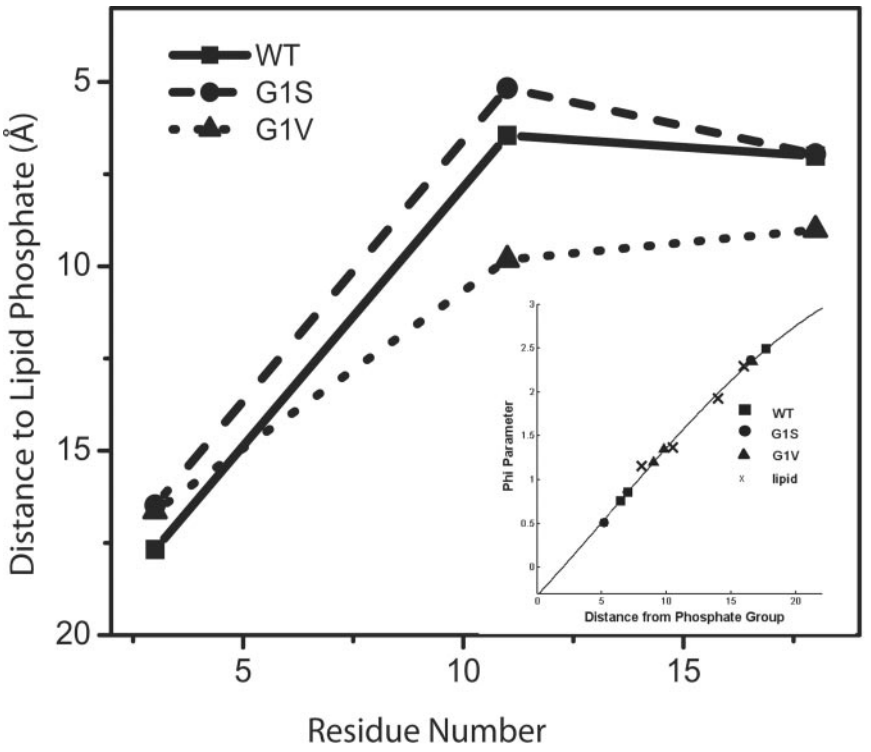

FIG. 4. Depth of three critical spin-labeled residues (Phe 3, Glu 11, and Ile 18) of wild-type, G1S, and G1V fusion domains in POPC:POPG (4:1) bilayers at pH 5. The depths were determined by fitting EPR spectra at increasing microwave powers in the presence of O_2, N_2, and NiEDDA to power saturation curves and ratioing the half-saturation powers in the presence of the different spin-relaxation agents as described in Materials and Methods. Inset: Best-fit calculated distances from NMR structures (abscissa) to experimental EPR depth parameters (ordinate) for wild-type, G1S, G1V, and four spin-labeled lipids used for depth calibration. All data fit the theoretical fitting function $\Phi = A\tanh[B(x - C] + D$, where A, B, C, and D are constants as described by Frazier et al. (19).

The depths in the lipid bilayer of the site-specific spin labels of the three molecules are shown in Fig. 4. G1S adopts a kinked structure very similar to that of the wild-type peptide in lipid bilayers, whereas G1V is more linear. The slight apparent bend of G1V is not intrinsic to the peptide but results from the fact that the side chain of Glu 11 projects from the opposite side of the linear helix than the side chains of Phe 3 and Ile 18 (Fig. 2D and G). Although Leu 2 at the N termini of all three structures penetrates the bilayer to approximately the same depth (17 to 19 Å), the linear and overall more hydrophobic G1V domain is more deeply buried in the bilayer. The irregular helix of G1V is oriented at an angle of 24 ± 7° to the plane of the membrane. This is less than the 38 ± 7° observed for the N-terminal arm of the wild-type structure. This difference is likely significant because the error estimates are based on assuming the most extreme cumulative depth errors and, therefore, were chosen very conservatively.

To visualize the fusion domains in lipid bilayers, we docked the NMR structures to the EPR depth constraints in fluid lipid bilayers (Fig. 5). The best fit calculated distances of the docked NMR structures fit the experimental EPR depth data very well (Fig. 4, inset). The high quality of these fits is a good indication that the structures of each of these domains must be similar in DPC micelles and fluid lipid bilayers, i.e., that the kinked G1S and the nonkinked G1V structures observed in DPC micelles are preserved in lipid bilayers. The similarity of the DPC and bilayer structures has been previously proven more rigorously, i.e., with 18 EPR data points, for the wild-type structures at pH 5 and 7.4 (26). Unfortunately it is impractical (and quite costly) to make 18 individual Cys mutants of each mutant by chemical synthesis. However, by extrapolation from the wild-type data, we assume that the matches of mutant structures in the two environments are of similar high quality as the matches of the wild-type structures in the two environments.

To gain further insight into the interaction of the wild-type and mutant fusion domains with lipid bilayers, we measured their secondary structures in fluid lipid bilayers by attenuated total reflection Fourier transform infrared spectroscopy as a function of their concentration in the membrane (Fig. 6). The wild-type peptide gave rise to only a single amide I′ band at ~1,650 cm^{-1} which is characteristic of α-helical (and possibly some irregular) secondary structures (48). When the concentration of G1S was increased to a high level, bands at ~1,628 and 1,685 cm^{-1} appeared, which indicate the presence of antiparallel β-sheet structures (48). Beta-sheet formation was much more dramatic for G1V and started at relatively moderate concentrations. The lipid concentrations (surface densities) in the supported bilayers did not change when the fusion domain concentrations were increased, as is evident from the approximately constant lipid ester carbonyl band at ~1,730 cm^{-1}. Thus, the wild-type fusion domain remains largely helical throughout the entire surface concentration range, but the mutants, particularly G1V, gradually convert to sizeable frac-

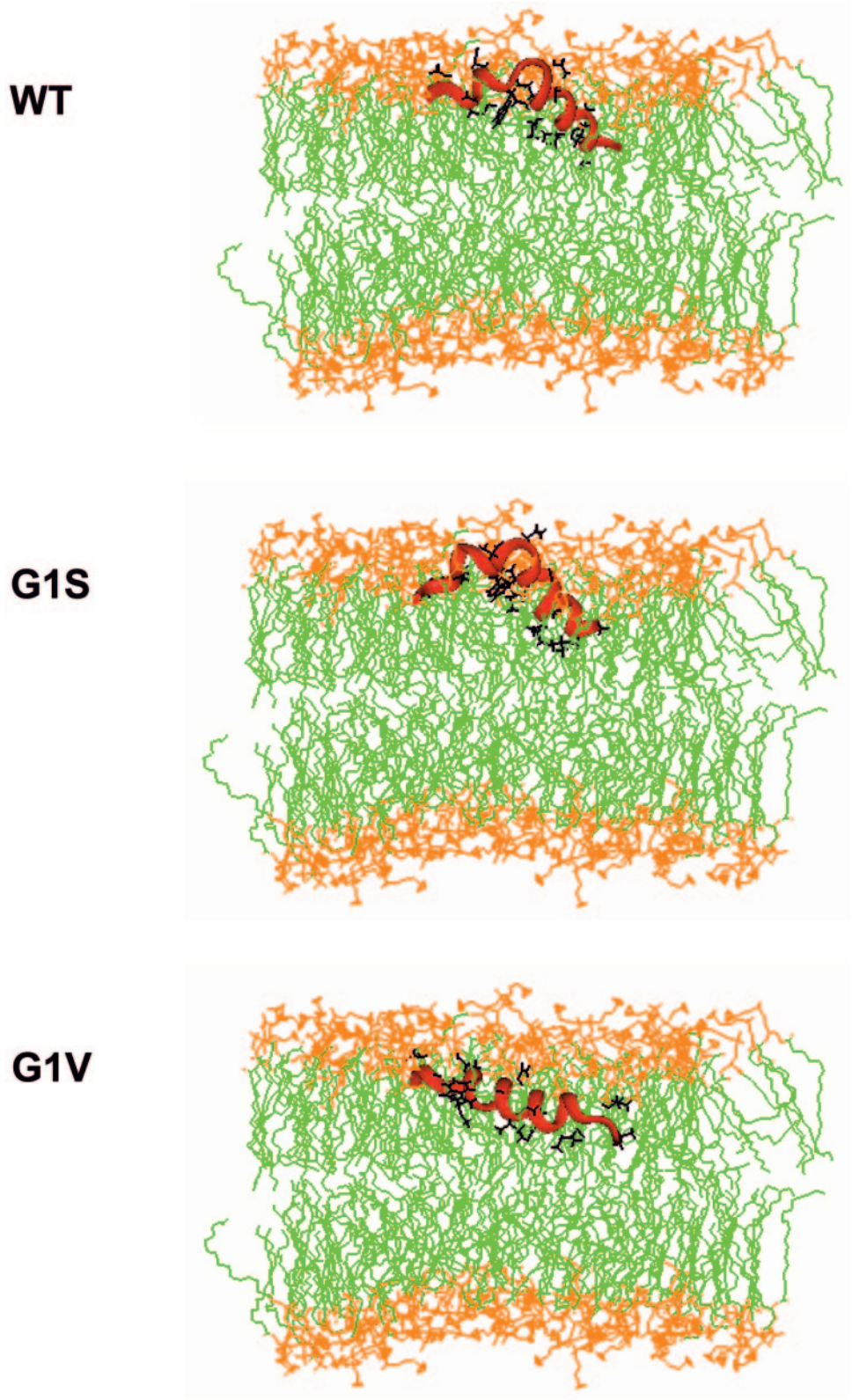

FIG. 5. Wild-type (WT), G1S, and G1V fusion domain structures docked to POPC bilayers using the experimental depth data of Fig. 4. C termini are on the left and N termini are on the right. The polar lipid head groups and glycerol backbones are shown in orange, and the aliphatic side chains are shown in green in the molecular dynamic-simulated lipid bilayers.

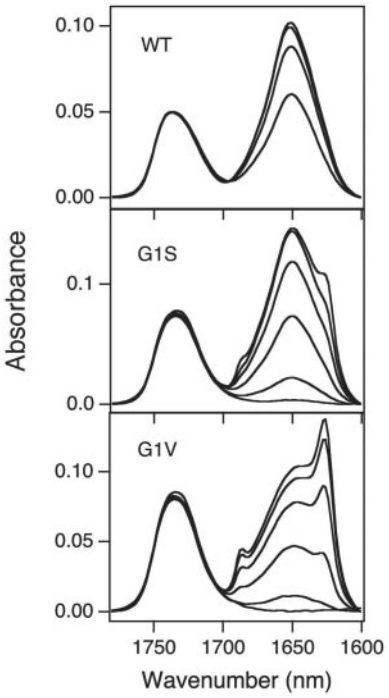

FIG. 6. ATR-FTIR spectra of wild-type, G1S, and G1V peptides bound to supported bilayers of POPC:POPG (4:1) at increasing concentrations at pH 5. Spectra were recorded after successive injections, from bottom to top, of 10, 20, 40, 80, and 100 μg/ml peptide and subsequent flushing of the cell with deuterium oxide buffer. The band at 1,735 cm^{-1} arises from the lipid ester carbonyl groups, and the complex band between 1,600 and 1,700 cm^{-1} is the amide I′ band from the bound fusion domains.

tions of antiparallel β-sheet as their surface concentrations are increased.

DISCUSSION

Implications of mutant fusion domain structures. The hydrophobic fusion domain at the N terminus of HA2 is one of the most conserved regions of influenza virus HA. The domain is the only portion of HA that inserts into target and perhaps viral membranes during membrane fusion (15). Therefore, it must be intimately involved in the fusion mechanism. The domain undergoes a dramatic conformational change when it is extruded from neutral-pH HA (52) and inserted into membranes at pH 5 (26). Our comparison of the NMR structures of the wild-type, G1S, and G1V domains in detergent micelles demonstrates that this domain is characterized by two critical features: an angle of about 105° at Asn 12 and a glycine ridge at the upper end of the N-terminal arm of the V- or boomerang-shaped molecule.

The boomerang is preserved in the hemifusion mutant G1S, but the N-terminal helix is slightly distorted. Most importantly, the serine side chain disrupts the smooth glycine ridge of the N-terminal helix in G1S. The boomerang structure is most likely preserved in lipid bilayer model membranes, as indicated by the site-directed spin labeling and polarized ATR-FTIR results. When docked into membranes, the N terminus points up towards the membrane interface and is presumably responsible for the slightly shallower location of the G1S structure compared to the wild-type structure in the membrane. The shallower location of G1S is paralleled by a free energy of binding to lipid bilayers that is 0.8 kcal/mol less negative than that of the wild-type fusion domain (33). Most of this free energy difference is enthalpic; the entropy change due to binding is almost the same for the G1S and wild-type fusion domains.

The fusion-blocking mutant G1V does not adopt the boomerang shape in detergent micelles or lipid bilayers. It is a linear molecule with a distorted α-helical structure that inserts into the membrane with a shallow tilt angle of approximately 24° from the membrane surface. (Polarized ATR-FTIR spectroscopy shows that G1V is oriented at about 10° from the membrane surface. We place more weight on the site-directed spin-labeled EPR experiment because the measurement is localized to the N-terminal helix, whereas the ATR-FTIR measurement considers the average orientation of all residues. Moreover, the EPR measurements are conducted in lipid vesicles, whereas the ATR-FTIR experiments are conducted in planar-supported membranes, which, even if fully hydrated, undergo fewer collective dynamic motions, such as, e.g., undulations, than bilayers in vesicles. Polarized ATR-FTIR spectra indicate average angles of 33° and 30° for the wild-type and G1S structures, respectively, from the membrane surface.)

Consistent with the NMR structure, circular dichroism spectroscopy also shows that G1V is about 35% less helical than the wild-type and G1S in detergent micelles and lipid bilayers (17). Although the amphiphilic G1V rod inserts into lipid bilayers as deeply as the wild-type and G1S boomerangs, its free energy of binding to lipid bilayers is only −5.8 kcal/mol, compared to −7.6 kcal/mol for binding of the wild-type structure to lipid bilayers (33). The binding of the wild-type and G1S structures is driven by a large favorable change in enthalpy but opposed by entropy. This mechanism of binding is known as the "nonclassical" hydrophobic effect. Although the binding of G1V to lipid bilayers is also driven by the nonclassical hydrophobic effect, the effect is not as dramatic: the enthalpy of binding of the wild-type structure is −16.5 kcal/mol compared to only −9.2 kcal/mol for G1V (33). Apparently, the wild-type and G1S boomerang structures "fit" better into the liquid crystalline structure of the lipid bilayer than the linear rod structure of G1V, leading to much larger enthalpic contributions to the total binding free energy. The "bad fit" of the G1V fusion domain in lipid bilayers is also the most likely reason for the dramatically increased propensity of G1V to aggregate into β-structures at higher surface concentrations (Fig. 6). This process is associated with a free energy of self-association of −3.5 kcal/mol (33).

It is rather unusual in soluble peptides that single-amino-acid changes at a terminus have such dramatic effects on their structures. However, terminal single-amino-acid changes can have quite far-reaching effects in membrane-bound peptides. The high thermodynamic cost of transferring the hydroxyl group of Ser 1 into the bilayer is avoided in G1S by forming a hydrogen bond between its oxygen and the backbone NH of Gly 4. As a result, the backbone CO of Ser 1 hydrogen bonds to the backbone NH of Ala 5 instead of Gly 4 as seen in the wild-type domain. Val 1 is rotated deep into the bilayer, which forces Phe 3 up towards the interface in G1V. These mem-

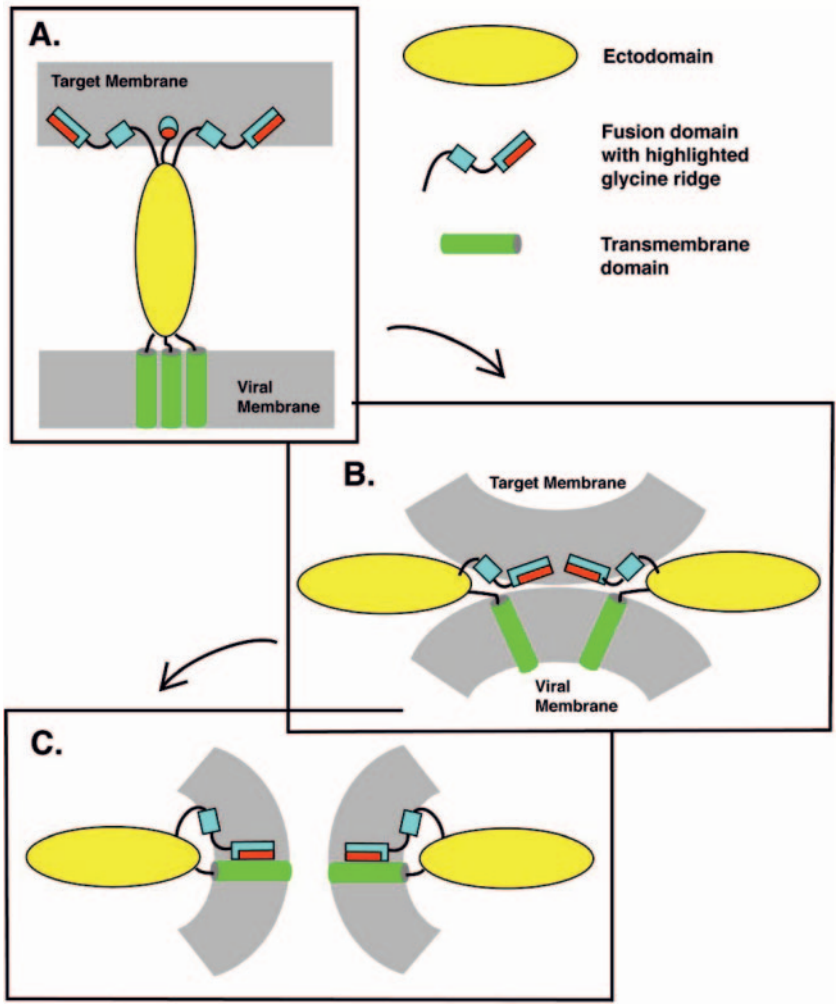

FIG. 7. Boomerang mechanism of influenza virus hemagglutinin-mediated membrane fusion. (A) The pH-induced spring-loaded conformational change in the ectodomain (6, 7) (not shown) thrusts the three boomerang-shaped fusion domains into the target membrane, where 7.6 kcal/mol of free energy is gained for each inserted domain. (B) The ectodomains tilt relative to the viral membrane plane (23, 49) and the boomerangs retrieve the target membrane and bring it into close juxtaposition with the viral membrane. The extended C-terminal "leashes" of the HA2 subunit pack into the grooves of the newly extended triple coiled coils at the N terminus and thereby bring the truncated N and C termini of HA2 into close proximity (9). Lipid exchange between the proximal leaflets, but not between the distal leaflets of the bilayer, can occur at this stage, which sometimes is also referred to as the hemifused state (10, 36). The boomerang shape of the fusion domain is required for the transition from A to B. For simplicity, only one fusion and one TM domain are shown, although it is known that three fusion and TM domains from several trimers all participate in a single fusion pore (4, 5, 13, 40). (C) In this model the fusion and TM domains interact by virtue of the glycine edge of the fusion domain to open the fusion pore. We hypothesize that once the proximal monolayers are sufficiently perturbed, the fusion domains latch onto the TM domains and glide down the TM domains. They thereby perturb not only the proximal but also the distal monolayers and thus open a first conductive fusion pore (39, 44). This event requires a TM domain that contains at least 17 hydrophobic residues (3) and a smooth glycine edge on the fusion domain (43). The fusion pore eventually dilates and permits unrestricted lipid flow in both leaflets of the bilayer. Again, only one fusion and one TM domain are shown for simplicity.

brane interactions disrupt some regular α-helical hydrogen bonds and position the helix more parallel to the membrane surface. Taken together, we conclude that the angle at Asn 12, i.e., the boomerang shape, is required for hemifusion and that a small residue (Gly or Ala) at the tip of the N-terminal arm of the boomerang is required to support full fusion.

Comparison with earlier work. In another recent ATR-FTIR study of G1S and G1V, G1V was found inserted into membranes as a perpendicular α-helix (18). We suspect that their very different results are due to differences in sample preparation. Epand et al. added fusion peptides in methanol to lipid bilayers and let them dry on germanium plates, whereas our EPR and ATR-FTIR measurements were conducted under physiological buffer conditions. We and others have shown previously that solvents can have dramatic effects on the structures of membrane-associated polypeptides and that the orientation of amphipathic peptides can be rotated by as much as 90° in suboptimally hydrated membranes (11, 20). We therefore believe that the perpendicular insertion of G1V that was observed by Epand et al. should be viewed with caution.

Fusion domain mutations may now be revisited on the basis of our new structural model in order to identify features that

might contribute to their activity. Gly 1, Phe 3, Ala 5, Ala 7, Gly 8, Phe 9, Glu 11, Gly 13, Trp 14, Gly 16, and Trp 21 of HA2 are absolutely conserved in all strains of influenza virus (14). This includes four glycines on the top and four aromatic residues that make up the hydrophobic pocket on the bottom of the molecule. Only conservative changes are permissible at Leu 2, Ile 10, Asn 12, Met 17, and Ile 18. Therefore, the amphipathic N-terminal helix and the ~105° angle formed by residues Glu 11, Asn 12, Gly 13, and Trp 14 are extremely well conserved, strongly supporting the notion that both structural elements are critical for activity not only in the peptide model system, but also in complete HA. Interestingly, the charged residues Glu 15 and Asp 19 and also Gly 20 in the C-terminal arm are relatively variable across different influenza virus strains, indicating that the top face of the C-terminal arm of the boomerang is less critical for fusion. The variability of Gly 4 and Ile 6 is puzzling and requires further investigation.

Proposed mechanism. The requirement for a smooth tip at the end of the glycine edge on the N-terminal arm raises interesting mechanistic questions about how the hemifusion intermediate progresses to full fusion. A glycine-rich surface on a membrane-inserted helix may be an ideal interface to interact with other helices in membranes. Glycophorin A, for example, forms a TM helix dimer through a motif that includes a blunt surface formed by Gly 79 and Gly 83 of one subunit juxtaposed to a bulky surface formed by Ile 76, Val 80, and Val 84 of the other subunit (35). Perhaps the fusion domain interacts with the TM domain of HA in a similar fashion. This scenario is supported by the fact that the TM domain of influenza virus HA promotes conversion of the hemifused to the fully fused state (3, 30, 37, 38). The finding that G1S and a mutant with a shortened TM domain exhibited the same hemifusion phenotype (3) is consistent with an interaction of these two domains at a late step in membrane fusion. A recently determined refined crystal structure of the low-pH conformation of the HA2 ectodomain also places the N- and C-terminal ends of the truncated HA2 chain and thus the (deleted) fusion and TM peptides in close proximity to each other (9).

Based on these observations, we suggest a mechanism for HA-mediated membrane fusion (Fig. 7). Our model is similar to previously proposed "cast-retrieve" models (55), but includes structural detail that has become available in the past several years. The neutral-pH structure of HA is metastable and spring-loaded (7). The pH change triggers the conformational change, which in turn propels the fusion domains toward the target membrane (6), where they insert by folding into the boomerang-shaped conformation (26). Tilting of the ectodomains pulls the target towards the viral membrane (23, 49). In this process, the C-terminal "leash" sequence of the ectodomain is redirected in a second conformational change towards the N terminus and gets packed into the groove between adjacent helices of the core coiled coils (9). The close juxtaposition of the two membranes and the lipid-perturbing effect of the fusion domains facilitate lipid exchange between the two proximal leaflets of the bilayers, which is phenomenologically equivalent to hemifusion. (The shape of the fusion domain does not in itself support negative membrane curvature, as has been hypothesized in some models of membrane fusion.)

Intra- or intermolecular interactions between the fusion and TM domains of HA promote the formation of an initial fusion pore (39, 44). This interaction may occur through the glycine edge of the N-terminal arm of the fusion domain and some unidentified residues of the TM domain. The N-terminal arm of the fusion domain is too short to penetrate the membrane completely. Therefore, it may slide down the TM domain and thereby open the fusion pore. This process may result in the "flickering" that is seen in electrophysiological recordings at the beginning of the opening of the fusion pore. Eventually the fusion pore dilates and becomes irreversibly opened, and lipids from both leaflets of the bilayer are free to flow across the expanded fusion pore (51, 54).

ACKNOWLEDGMENT

This work was supported by National Institutes of Health grant AI30557.

REFERENCES

1. **Altenbach, C., D. A. Greenhalgh, H. G. Khorana, and W. L. Hubbell.** 1994. A collision gradient method to determine the immersion depth of nitroxides in lipid bilayers: application to spin-labeled mutants of bacteriorhodopsin. Proc. Natl. Acad. Sci. USA **91:**1667–1671.
2. **Ames, B. N.** 1966. Assays of inorganic phosphate, total phosphate and phosphatases. Methods Enzymol. **8:**115–118.
3. **Armstrong, R. T., A. S. Kushnir, and J. M. White.** 2000. The transmembrane domain of influenza hemagglutinin exhibits a stringent length requirement to support the hemifusion to fusion transition. J. Cell Biol. **151:**425–437.
4. **Bentz, J.** 2000. Minimal aggregate size and minimal fusion unit for the first fusion pore of influenza hemagglutinin-mediated membrane fusion. Biophys. J. **78:**227–245.
5. **Blumenthal, R., D. P. Sarkar, S. Durell, D. E. Howard, and S. J. Morris.** 1996. Dilation of the influenza hemagglutinin fusion pore revealed by the kinetics of individual cell-cell fusion events. J. Cell Biol. **135:**63–71.
6. **Bullough, P. A., F. M. Hughson, J. J. Skehel, and D. C. Wiley.** 1994. Structure of influenza haemagglutinin at the pH of membrane fusion. Nature **371:**37–43.
7. **Carr, C. M., C. Chaudhry, and P. S. Kim.** 1997. Influenza hemagglutinin is spring-loaded by a metastable native conformation. Proc. Natl. Acad. Sci. USA **94:**14306–14313.
8. **Carr, C. M., and P. S. Kim.** 1993. A spring-loaded mechanism for the conformational change of influenza hemagglutinin. Cell **73:**823–832.
9. **Chen, J., J. J. Skehel, and D. C. Wiley.** 1999. N- and C-terminal residues combine in the fusion-pH influenza hemagglutinin HA(2) subunit to form an N cap that terminates the triple-stranded coiled coil. Proc. Natl. Acad. Sci. USA **96:**8967–8972.
10. **Chernomordik, L. V., V. A. Frolov, E. Leikina, P. Bronk, and J. Zimmerberg.** 1998. The pathway of membrane fusion catalyzed by influenza hemagglutinin: restriction of lipids, hemifusion, and lipidic fusion pore formation. J. Cell Biol. **140:**1369–1382.
11. **Cross, T. A., A. Arseniev, B. A. Cornell, J. H. Davis, J. A. Killian, R. E. Koeppe, 2nd, L. K. Nicholson, F. Separovic, and B. A. Wallace.** 1999. Gramicidin channel controversy–revisited. Nat. Struct. Biol. **6:**610–611; discussion 611–612.
12. **Dalton, L. A., J. O. McIntyre, and S. Fleischer.** 1987. Distance estimate of the active center of D-beta-hydroxybutyrate dehydrogenase from the membrane surface. Biochemistry **26:**2117–2130.
13. **Danieli, T., S. L. Pelletier, Y. I. Henis, and J. M. White.** 1996. Membrane fusion mediated by the influenza virus hemagglutinin requires the concerted action of at least three hemagglutinin trimers. J. Cell Biol. **133:**559–569.
14. **Durell, S. R., I. Martin, J. M. Ruysschaert, Y. Shai, and R. Blumenthal.** 1997. What studies of fusion peptides tell us about viral envelope glycoprotein-mediated membrane fusion (review). Mol. Membr. Biol. **14:**97–112.
15. **Durrer, P., C. Galli, S. Hoenke, C. Corti, R. Gluck, T. Vorherr, and J. Brunner.** 1996. H^+-induced membrane insertion of influenza virus hemagglutinin involves the HA2 amino-terminal fusion peptide but not the coiled coil region. J. Biol. Chem. **271:**13417–13421.
16. **Earp, L. J., S. E. Delos, H. E. Park, and J. M. White.** 2004. The many mechanisms of viral membrane fusion proteins. Curr. Top. Microbiol. Immunol. **285:**25–66.
17. **Eckert, D. M., and P. S. Kim.** 2001. Mechanisms of viral membrane fusion and its inhibition. Annu. Rev. Biochem. **70:**777–810.
18. **Epand, R. M., R. F. Epand, I. Martin, and J. M. Ruysschaert.** 2001. Membrane interactions of mutated forms of the influenza fusion peptide. Biochemistry **40:**8800–8807.
19. **Frazier, A. A., M. A. Wisner, N. J. Malmberg, K. G. Victor, G. E. Fanucci, E. A. Nalefski, J. J. Falke, and D. S. Cafiso.** 2002. Membrane orientation and position of the C2 domain from cPLA2 by site-directed spin labeling. Biochemistry **41:**6282–6292.

20. **Frey, S., and L. K. Tamm.** 1991. Orientation of melittin in phospholipid bilayers. A polarized attenuated total reflection infrared study. Biophys. J. **60:**922–930.
21. **Gething, M. J., R. W. Doms, D. York, and J. White.** 1986. Studies on the mechanism of membrane fusion: site-specific mutagenesis of the hemagglutinin of influenza virus. J. Cell Biol. **102:**11–23.
22. **Gibbons, D. L., M. C. Vaney, A. Roussel, A. Vigouroux, B. Reilly, J. Lepault, M. Kielian, and F. A. Rey.** 2004. Conformational change and protein-protein interactions of the fusion protein of Semliki Forest virus. Nature **427:**320–325.
23. **Gray, C., and L. K. Tamm.** 1998. pH-induced conformational changes of membrane-bound influenza hemagglutinin and its effect on target lipid bilayers. Protein Sci. **7:**2359–2373.
24. **Guntert, P., W. Braun, and K. Wuthrich.** 1991. Efficient computation of three-dimensional protein structures in solution from nuclear magnetic resonance data using the program DIANA and the supporting programs CALIBA, HABAS and GLOMSA. J. Mol. Biol. **217:**517–530.
25. **Guntert, P., C. Mumenthaler, and K. Wuthrich.** 1997. Torsion angle dynamics for NMR structure calculation with the new program DYANA. J. Mol. Biol. **273:**283–298.
26. **Han, X., J. H. Bushweller, D. S. Cafiso, and L. K. Tamm.** 2001. Membrane structure and fusion-triggering conformational change of the fusion domain from influenza hemagglutinin. Nat. Struct. Biol. **8:**715–720.
27. **Han, X., D. A. Steinhauer, S. A. Wharton, and L. K. Tamm.** 1999. Interaction of mutant influenza virus hemagglutinin fusion peptides with lipid bilayers: probing the role of hydrophobic residue size in the central region of the fusion peptide. Biochemistry **38:**15052–15059.
28. **Han, X., and L. K. Tamm.** 2000. A host-guest system to study structure-function relationships of membrane fusion peptides. Proc. Natl. Acad. Sci. USA **97:**13097–13102.
29. **Han, X., and L. K. Tamm.** 2000. pH-dependent self-association of influenza hemagglutinin fusion peptides in lipid bilayers. J. Mol. Biol. **304:**953–965.
30. **Kemble, G. W., T. Danieli, and J. M. White.** 1994. Lipid-anchored influenza hemagglutinin promotes hemifusion, not complete fusion. Cell **76:**383–391.
31. **Lai, A. L., Y. Li, and L. K. Tamm.** Interplay of proteins and lipids in virus entry by membrane fusion, p. 279–305. *In* L. K. Tamm (ed.), Protein-lipid interactions, in press. Wiley-VCH, Weinheim, Germany.
32. **Langen, R., K. J. Oh, D. Cascio, and W. L. Hubbell.** 2000. Crystal structures of spin labeled T4 lysozyme mutants: implications for the interpretation of EPR spectra in terms of structure. Biochemistry **39:**8396–8405.
33. **Li, Y., X. Han, and L. K. Tamm.** 2003. Thermodynamics of fusion peptide-membrane interactions. Biochemistry **42:**7245–7251.
34. **Luginbuhl, P., P. Guntert, M. Billeter, and K. Wuthrich.** 1996. The new program OPAL for molecular dynamics simulations and energy refinements of biological macromolecules. J. Biomol. NMR **8:**136–146.
35. **MacKenzie, K. R., J. H. Prestegard, and D. M. Engelman.** 1997. A transmembrane helix dimer: structure and implications. Science **276:**131–133.
36. **Melikyan, G. B., S. A. Brener, D. C. Ok, and F. S. Cohen.** 1997. Inner but not outer membrane leaflets control the transition from glycosylphosphatidylinositol-anchored influenza hemagglutinin-induced hemifusion to full fusion. J. Cell Biol. **136:**995–1005.
37. **Melikyan, G. B., H. Jin, R. A. Lamb, and F. S. Cohen.** 1997. The role of the cytoplasmic tail region of influenza virus hemagglutinin in formation and growth of fusion pores. Virology **235:**118–128.
38. **Melikyan, G. B., S. Lin, M. G. Roth, and F. S. Cohen.** 1999. Amino acid sequence requirements of the transmembrane and cytoplasmic domains of influenza virus hemagglutinin for viable membrane fusion. Mol. Biol. Cell **10:**1821–1836.
39. **Melikyan, G. B., R. M. Markosyan, M. G. Roth, and F. S. Cohen.** 2000. A point mutation in the transmembrane domain of the hemagglutinin of influenza virus stabilizes a hemifusion intermediate that can transit to fusion. Mol. Biol. Cell **11:**3765–3775.
40. **Melikyan, G. B., W. D. Niles, and F. S. Cohen.** 1995. The fusion kinetics of influenza hemagglutinin expressing cells to planar bilayer membranes is affected by HA density and host cell surface. J. Gen. Physiol. **106:**783–802.
41. **Modis, Y., S. Ogata, D. Clements, and S. C. Harrison.** 2004. Structure of the dengue virus envelope protein after membrane fusion. Nature **427:**313–319.
42. **Pecheur, E. I., J. Sainte-Marie, A. Bienven e, and D. Hoekstra.** 1999. Peptides and membrane fusion: towards an understanding of the molecular mechanism of protein-induced fusion. J. Membr. Biol. **167:**1–17.
43. **Qiao, H., R. T. Armstrong, G. B. Melikyan, F. S. Cohen, and J. M. White.** 1999. A specific point mutant at position 1 of the influenza hemagglutinin fusion peptide displays a hemifusion phenotype. Mol. Biol. Cell **10:**2759–2769.
44. **Schoch, C., and R. Blumenthal.** 1993. Role of the fusion peptide sequence in initial stages of influenza hemagglutinin-induced cell fusion. J. Biol. Chem. **268:**9267–9274.
45. **Skehel, J. J., and D. C. Wiley.** 1998. Coiled coils in both intracellular vesicle and viral membrane fusion. Cell **95:**871–874.
46. **Skehel, J. J., and D. C. Wiley.** 2000. Receptor binding and membrane fusion in virus entry: the influenza hemagglutinin. Annu. Rev. Biochem. **69:**531–569.
47. **Tamm, L. K., and X. Han.** 2000. Viral fusion peptides: a tool set to disrupt and connect biological membranes. Biosci. Rep. **20:**501–518.
48. **Tamm, L. K., and S. A. Tatulian.** 1997. Infrared spectroscopy of proteins and peptides in lipid bilayers. Q. Rev. Biophys. **30:**365–429.
49. **Tatulian, S. A., P. Hinterdorfer, G. Baber, and L. K. Tamm.** 1995. Influenza hemagglutinin assumes a tilted conformation during membrane fusion as determined by attenuated total reflection FTIR spectroscopy. EMBO J. **14:**5514–5523.
50. **Tieleman, D. P., H. J. Berendsen, and M. S. Sansom.** 2001. Voltage-dependent insertion of alamethicin at phospholipid/water and octane/water interfaces. Biophys. J. **80:**331–346.
51. **Tse, F. W., A. Iwata, and W. Almers.** 1993. Membrane flux through the pore formed by a fusogenic viral envelope protein during cell fusion. J. Cell Biol. **121:**543–552.
52. **Wilson, I. A., J. J. Skehel, and D. C. Wiley.** 1981. Structure of the haemagglutinin membrane glycoprotein of influenza virus at 3 A resolution. Nature **289:**366–373.
53. **Wishart, D. S., B. D. Sykes, and F. M. Richards.** 1992. The chemical shift index: a fast and simple method for the assignment of protein secondary structure through NMR spectroscopy. Biochemistry **31:**1647–1651.
54. **Zimmerberg, J., R. Blumenthal, D. P. Sarkar, M. Curran, and S. J. Morris.** 1994. Restricted movement of lipid and aqueous dyes through pores formed by influenza hemagglutinin during cell fusion. J. Cell Biol. **127:**1885–1894.
55. **Zimmerberg, J., S. S. Vogel, and L. V. Chernomordik.** 1993. Mechanisms of membrane fusion. Annu. Rev. Biophys. Biomol. Struct. **22:**433–466.